Simultaneous detection of ultraviolet and infrared radiation in a single GaN/GaAlN heterojunction

Ranga C. Jayasinghe,[1] Gamini Ariyawansa,[1] Nikolaus Dietz,[1] A. G. Unil Perera,[1,2,*] Steven G. Matsik,[2] Hongbo B. Yu,[3] Ian T. Ferguson,[3] Andrew Bezinger,[4] Sylvain R. Laframboise,[4] Margaret Buchanan,[4] and Hui Chun Liu[4]

[1]*Department of Physics and Astronomy, Georgia State University, Atlanta, Georgia 30303, USA*
[2]*NDP Optronics LLC, Mableton, Georgia 30126, USA*
[3]*School of Electrical and Computer Engineering, Georgia Institute of Technology, Atlanta, Georgia 30332, USA*
[4]*Institute for Microstructural Sciences, National Research Council, Ottawa K1A 0R6, Canada*
**Corresponding author: uperera@gsu.edu*

Received June 20, 2008; revised August 14, 2008; accepted August 19, 2008;
posted September 18, 2008 (Doc. ID 97762); published October 17, 2008

Results are presented for a dual-band detector that simultaneously detects UV radiation in the 250–360 nm and IR radiation in the 5–14 μm regions with near zero spectral cross talk. In this detector having separate UV- and IR-active regions with three contacts (one common contact for both regions) allows the separation of the UV and IR generated photocurrent components, identifying the relative strength of each component. This will be an important development in UV–IR dual-band applications such as fire–flame detection, solar astronomy, and military sensing, eliminating the difficulties of employing several individual detectors with separate electronics–cooling mechanisms. © 2008 Optical Society of America

OCIS codes: 040.3060, 040.5160, 040.7190, 230.0040, 230.0250, 250.0040.

UV–IR dual-band photodetectors have potential applications in various areas, such as fire–flame detection [1], solar astronomy, military sensing, situational awareness applications, and combustion process monitoring [2,3]. Since the UV–IR dual-band detectors do not respond to solar radiation or another artificial visible lighting, the false detection rate is strongly reduced. Dual-band detectors operating in the near-, mid-, and far-IR regions based on the group III-As material [4–7] systems have been previously reported. In the dual-band detector reported [8] before, both photocurrent components were collected from the same two terminals. This limits the usefulness of the detector due to the inability of determining which wavelength was detected (UV, IR, or both). The dual-band detector reported here has separate UV- and IR-active regions with three contacts (one common contact for both regions) for separate and simultaneous measurements of the UV- and IR-photocurrent components. This concept has been predicted before for a GaN/AlGaN heterostructure [9]. It was experimentally investigated, and the results are reported in this Letter.

The structure [see Fig. 1(a)] consists of an n^+-GaN top-contact (TC) layer, an undoped $Ga_{0.974}Al_{0.026}N$ layer acting as the UV-active region, an n^+-GaN middle-contact (MC) layer, the IR-active region, and a bottom-contact (BC) layer. The IR-active region consists of two periods of an n^+-GaN emitter layer and an undoped $Ga_{0.974}Al_{0.026}N$ barrier layer. Depending on the bias either the MC or the BC also acts as an emitter. The epitaxial layers were grown by low pressure metal-organic chemical-vapor deposition (MOCVD) on a c-plane sapphire substrate. The devices were processed by dry etching technique, and ring contacts were made by depositing Ti/Al/Ti/Au [300/800/1200/550 Å]. The electrical and optical areas of the device are 400 μm $\times$ 400 μm and 270 μm $\times$ 270 μm, respectively.

The dual-band detection is based on two absorption mechanisms in the heterostructure. Interband absorption in the top $Ga_{0.974}Al_{0.026}N$ layer producing electron–hole pairs, which are then swept out by an external electric field and collected at the contacts, is the basis for the UV detection with a wavelength threshold corresponding to the bandgap of the $Ga_{0.974}Al_{0.026}N$ layer. The IR response is due to free carrier absorption in the emitters and internal photoemission over the barriers followed by carrier collec-

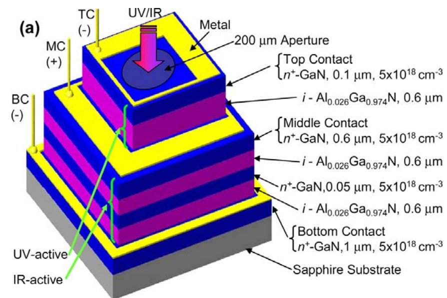

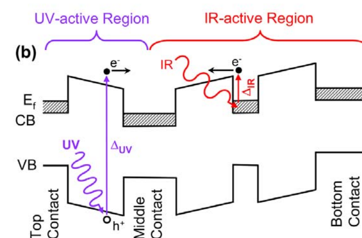

Fig. 1. (Color online) Three contact structure for simultaneous dual-band response measurements showing (a) separate active regions for UV and IR measurements and (b) the corresponding band diagram (CB and VB are the conduction and valence bands, respectively) under reverse bias configuration. The labels TC, MC, and BC indicate the top, middle, and bottom contacts, respectively; and (+) or (−) show the relative potential at which the device was operated. A 200 μm aperture was used to block the radiation leakage through the outer openings to the IR-active region.

 © 2008 Optical Society of America

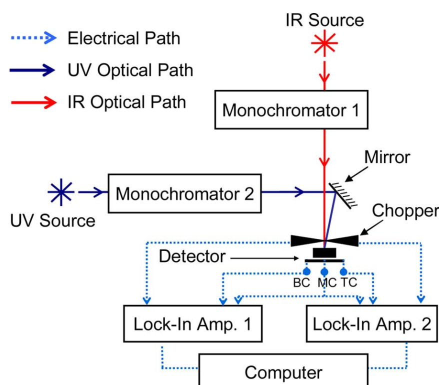

Fig. 2. (Color online) Experimental setup for measuring the UV and IR components simultaneously. A single optical chopper is used to modulate the incoming radiation, as in a typical application.

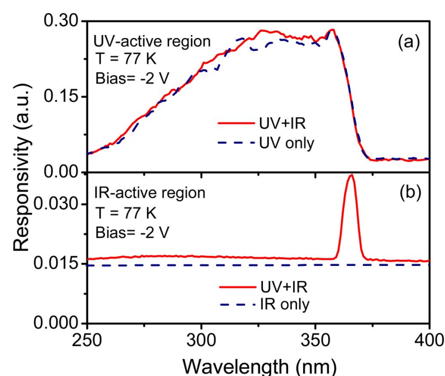

Fig. 3. (Color online) Simultaneously measured photocurrents (solid curves) from (a) the UV-active region (TC-MC) and (b) the IR-active region (MC-BC) at 77 K when both UV and IR radiations were incident onto the detector. The UV wavelength was varied between 250–400 nm, while IR was fixed at 9.3 μm (using a CO_2 laser). The dashed curve in (a) represents the photocurrent when only UV radiation was incident and the dashed line in (b) indicates the level of the IR-active region response when only IR radiation was incident.

tion at the contacts using an external electric field. The IR response wavelength threshold corresponds to the interfacial work function Δ, which arises due to the band offset of different materials [10] and the bandgap narrowing [11] of the n^+-GaN emitter layer. The thresholds for the UV and IR responses can be controlled separately by using $Ga_{1-y}Al_yN$ emitters and $Ga_{1-x}Al_xN$ barriers. Thus, by adjusting the Al fraction in the barrier [9] (x) both the UV and IR thresholds can be changed, and adjusting the Al fraction in the emitter (y) allows the IR threshold to be tailored without changing the UV threshold. Adjusting both x and y, it is also possible to change the UV threshold without changing the IR threshold.

Throughout this discussion, the MC terminal is the common terminal for both UV- and IR-active regions. Hence, forward (reverse) bias denotes that the TC for the UV-active region or the BC for the IR-active region is positive (negative) relative to the MC. When the TC is negatively biased, it also acts as an emitter, making the IR detection possible in the UV-active region. This effect can be decreased by reducing the TC layer thickness, which reduces the IR absorption and the generated photocurrent. Furthermore, this TC layer absorbs UV radiation, suppressing the transmission of UV into the UV-active region, without generating photocurrent, because the excited electron–hole pairs are trapped by the barriers and recombine in the highly doped TC. For an optimum UV response, the TC layer thickness was found to be 0.1 μm, which is thin enough to reduce the IR absorption while still giving uniform electric field distribution across the UV-active region. Furthermore, the generation of IR photocurrent is prominent in the IR-active region, while no UV photocurrent is expected irrespective of the bias configuration, since almost all the UV radiation is absorbed within the UV-active region.

For simultaneous UV and IR photocurrent measurement with a near zero spectral cross talk, the direction of the applied electric field across each region should be determined. As explained before a UV photocurrent from the UV-active region is expected for both forward and reverse bias configurations, while an IR photocurrent from the UV-active region is not expected under reverse bias. From the IR-active region, an IR photocurrent is expected for both forward and reverse bias, while no UV photocurrent is expected under any bias configuration. Hence, for simultaneous dual-band detection, the UV- and IR-active regions should be under reverse bias configuration as shown in Fig. 1(b). Under this configuration, the majority carriers move toward the MC, and would not cross from one active region into the other.

In the spectral measurement setup, an optical chopper (see Fig. 2) was used to modulate both the UV and IR radiations, providing the same modulation as in a typical application. A 200-μm-diameter aperture [as shown in Fig. 1(a)] was used to block the UV radiation leakage (i.e., entering the IR-active region without passing through the UV-active region) through the region around the MC. The responses from both active regions were obtained simultaneously at 77 K as shown in Fig. 3. The UV spectra were obtained by using a Deuterium UV source, DK480 monochromator, and neutral density filters. The UV spectra were calibrated using a background spectrum obtained by a Hamamatsu photomultiplier

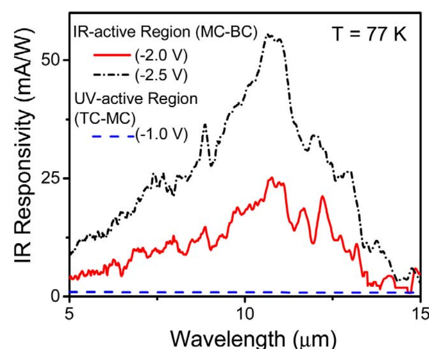

Fig. 4. (Color online) IR response from IR- and UV-active regions at 77 K. The UV-active region showed almost zero response for IR radiation under reverse bias configuration as expected.

Table 1. Response for Different Combinations of Incident Radiation[a]

	UV-Active Region (TC-MC)		IR-Active Region (MC-BC)	
	With UV (mV)	Without UV (mV)	With UV (mV)	Without UV (mV)
With IR	6.0	0.0	1.5	1.4
Without IR	6.0	0.0	0.1	0.0

[a]The wavelengths were held constant at 300 nm for UV and 9.3 μm for IR. The results were left as voltage signals for a fixed load resistor.

tube with a known sensitivity. A CO_2 laser at 9.3 μm with 0.1 W output power was used as the IR source. The solid curves show simultaneously measured photocurrents from the UV-active region [Fig. 3(a)] and the IR-active region [Fig. 3(b)] at 77 K when both IR and UV radiations were incident onto the detector. The UV wavelength was varied between 250–400 nm (x axis of the figure), while IR radiation was fixed at 9.3 μm (using the CO_2 laser). The dashed curve in Fig. 3(a) represents the photocurrent from the UV-active region when only the UV radiation was incident. Comparing the two curves, it is evident that there is no significant effect from IR radiation on the response, indicating a sole UV detection from the UV-active region. The nearly constant response from the IR-active region, which is almost equal to the pure IR response [dashed line in Fig. 3(b)], is a good indication that the response is due to the fixed IR light (9.3 μm) and there is no effect from the UV radiation except for an exciton peak observed around 365 nm. The broad IR responses from both active regions obtained separately at 77 K are shown in Fig. 4, with the free carrier response seen as a broad peak with a maximum near 11 μm. The UV-active region did not show a measurable IR response under negative bias but did show a response under positive bias as expected.

For the IR-active region, a response feature at ~365 nm is observed, which is probably due to one of the following two reasons: (i) it could be due to a light transmission as a result of a generation-recombination mechanism of an exciton [12]. An exciton (~365 nm) generated in the top GaAlN layer in the UV-active region could relax re-emitting a UV photon, generating another exciton, and so on, allowing a small fraction of photons at ~365 nm to pass through to the IR-active region; (ii) the low energy UV radiation that has energy below the bandgap of $Ga_{0.974}Al_{0.026}N$ was absorbed in the MC layer, and the generated photocurrent could be either due to the minority carrier transportation [13] in the structure where the generated holes were recombined with the electrons in the valence band, or electron hopping from the filled impurity acceptor levels above the valence band of GaAlN layers. However, further studies are needed to verify these ideas.

In an ideal dual-band detector, the UV response should be obtained solely from the UV-active region and the IR response from the IR-active region. Tests were carried out varying the combination of incident radiation while keeping the UV wavelength fixed at 300 nm and the IR wavelength fixed at 9.3 μm. As given in Table 1, the results are listed as voltage signals for fixed load resistor values, showing no effect from IR radiation on the response from the UV-active region and a near noise level change in the response from the IR-active region by UV radiation (i.e., near zero spectral cross talk).

In conclusion, results have been presented for a GaN/GaAlN single element detector capable of simultaneously identifying both the UV (250–360 nm) and IR (5–14 μm) responses with near zero spectral cross talk. The detector consists of separate UV- and IR-active regions with separate electrical contacts. The detector can be further improved by the addition of more periods of GaN/GaAlN in the IR-active region and using interdigitated contacts in the UV-active region.

This work was supported in part by the U.S. Air Force Small Business Innovation Research (SBIR) Program under grant FA9453-05-M-0106. The authors thank Dave Cardimona and Bill Glass for fruitful discussions.

References

1. D. Starikov, C. Boney, R. Pillai, and A. Bensaoula, in *Proceedings of the ISA/IEEE Sensors for Industry Conference* (IEEE, 2004), pp. 36–40.
2. M. A. Khan, J. N. Kuznia, D. T. Olson, M. Blasingame, and A. R. Bhattarai, Appl. Phys. Lett. **63**, 2455 (1993).
3. D. Walker, X. Zhang, P. Kung, A. Saxler, S. Javadpour, J. Xu, and M. Razeghi, Appl. Phys. Lett. **68**, 2100 (1996).
4. G. Ariyawansa, M. B. M. Rinzan, D. G. Esaev, S. G. Matsik, G. Hastings, A. G. U. Perera, H. C. Liu, B. N. Zvonkov, and V. I. Gavrilenko, Appl. Phys. Lett. **86**, 143510 (2005).
5. A. Goldberg, P. N. Uppal, and M. Winn, Infrared Phys. Technol. **44**, 427 (2003).
6. H. C. Liu, C. Y. Song, A. Shen, M. Gao, Z. R. Wasilewski, and M. Buchanan, Appl. Phys. Lett. **77**, 2437 (2000).
7. M. P. Touse, G. Karunasiri, K. R. Lantz, H. Li, and T. Mei, Appl. Phys. Lett. **86**, 093501 (2005).
8. G. Ariyawansa, M. B. M. Rinzan, M. Alevli, M. Strassburg, N. Dietz, A. G. U. Perera, S. G. Matsik, A. Asghar, I. T. Ferguson, H. Luo, A. Bezinger, and H. C. Liu, Appl. Phys. Lett. **89**, 091113 (2006).
9. A. G. U. Perera, G. Ariyawansa, M. B. M. Rinzan, M. Stevens, M. Alevli, N. Dietz, S. G. Matsik, A. Asghar, I. T. Ferguson, H. Luo, A. Bezinger, and H. C. Liu, Infrared Phys. Technol. **50**, 142 (2007).
10. D. G. Esaev, M. B. M. Rinzan, S. G. Matsik, and A. G. U. Perera, J. Appl. Phys. **96**, 4588 (2004).
11. W. Z. Shen, A. G. U. Perera, H. C. Liu, M. Buchanan, and W. J. Schaff, Appl. Phys. Lett. **71**, 2677 (1997).
12. H. Jiang, G. Y. Zhao, H. Ishikawa, T. Egawa, T. Jimbo, and M. Umeno, J. Appl. Phys. **89**, 1046 (2001).
13. L. Chernyak, A. Osinsky, and A. Schultea, Solid-State Electron. **45**, 1687 (2001).